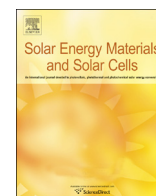




ELSEVIER

Contents lists available at SciVerse ScienceDirect

Solar Energy Materials & Solar Cells

journal homepage: www.elsevier.com/locate/solmat

Growth of vertically aligned ZnO nanowalls for inverted polymer solar cells

Zhiqiang Liang^{a,b}, Rui Gao^b, Jo-Lin Lan^b, Orawan Wiranwetchayan^b, Qifeng Zhang^b,
Chundong Li^{a,*}, Guozhong Cao^{b,*}^a School of Material Science and Engineering, Harbin Institute of Technology, Harbin 150001, PR China^b Department of Materials Science and Engineering, University of Washington, Seattle, WA 98195, USA

ARTICLE INFO

Article history:

Received 30 November 2012

Received in revised form

8 May 2013

Accepted 9 May 2013

Keywords:

Inverted polymer solar cells

Zinc oxide

Nanowalls

Aqueous solution growth

ABSTRACT

This paper reports a facile fabrication of vertical ZnO nanowalls on ITO coated glass substrates by using an aqueous solution growth method at low temperature. The formation of nanowalls is ascribed to selective dissolution of (001) planes of the chemical bath deposited dense ZnO rods. The morphology of the etched ZnO nanowalls is determined by the structure of the as-grown ZnO rod arrays, which can be readily controlled by tuning aqueous solution parameters such as: initial pH value of chemical bath solution and the growth temperature. With vertically aligned ZnO nanowalls as electrode in inverted polymer solar cells, the average performance of devices with open circuit voltage, short circuit current density, fill factor, and power conversion efficiency are measured as 0.56 V, 7.56 mW cm⁻², 0.49 and 2.14%, respectively. The results indicate that the two-dimensional structure of ZnO nanowalls can effectively serve as an electrode for inverted polymer solar cells.

© 2013 Elsevier B.V. All rights reserved.

1. Introduction

Inverted polymer solar cells (PSCs) using n-type inorganic metal oxide nanostructures as electrode have attracted considerable attentions because of it has improved ambient device stability and compatibility to all solution roll-to-roll type fabrication onto flexible based substrates [1–5]. ZnO are particularly well-suited for this application because it has good transparency in the whole visible range, relatively high electron mobility, environment friendly and low-cost [6–9]. In addition, ZnO thin film can be easily processed via many methods at relatively low temperature, making ZnO fully compatible with fabrication onto flexible substrates [5,10–13]. It is known that the ZnO is the only material as cathode buffer layer that has been widely used in inverted PSCs and fabricated by roll-to-roll processing technique [14–16]. Recently, one dimensional (1D) ZnO nanostructures have attracted a lot of studies for applications in inverted PSCs [17–25]. The air stable vertically aligned 1D metal oxide could improve the performance of the inverted polymer solar cells by providing a short and continuous pathway for electron transport and might additionally contribute to enhancing the exciton dissociation ratio [19,24]. However, the solar cells with vertically aligned 1D ZnO nanostructures and P3HT:PCBM blend exhibited PCEs around

only 2%, with a few exceptions reached 3%–4% [21–25]. Ajuria et al. [24] had yielded a PCE up to 4.1% by improving the contact quality between ZnO and P3HT:PCBM layer and enhancing the ZnO/active layer interface area, which was obtained by using the ZnO nanoparticles modified ZnO nanowire arrays, a strong indication that a higher specific surface does promote the performance of the inverted PSCs. It has been demonstrated and explained that the performance of the inverted PSCs can be promoted by increasing the ZnO/active layer interface area [8,24,26].

ZnO nanowalls (NWs), as a two-dimensional (2D) nanostructure with larger surface area than 1D nanostructure, hold a high potential for application in inverted PSCs. The application of ZnO nanorods in inverted PSCs has attracted a lot of investigations. However, there is little or no report on the application of ZnO NWs in inverted PSCs. Recently, Shin et al. reported that the application of ZnO NWs as electron transport and hole block layers can enhance the PCE of inverted organic solar cells due to the increase in the charge transport interface area [27]. Our work will evidently serve three purposes: (1) supporting and verifying this most recent publication, (2) offering an alternative morphology and possibly different surface chemistry, and (3) promising a further study on the manipulation of morphology and surface chemistry for better power conversion efficiency and better fundamental understanding.

Because the ZnO NWs have high potential for application in many fields, such as: energy-storage devices [28], biological sensors [29,30], and field emission (FE) [31], in the past decade, the ZnO NWs structures have been achieved by many methods at

* Corresponding authors.

E-mail address: gzciao@u.washington.edu (G. Cao).

high growth temperature (500 °C–1100 °C) under vacuum and/or with catalyst [28–30,32–36]. High growth temperatures limit the applicable substrate materials, such as the transparent conducting oxides (TCOs) substrates which are usually used as transparent electrodes in the application of photovoltaics and opto-electronics devices, since the conductivity of TCO usually decays rapidly at high annealing temperatures of above 500 °C [37]. Recently, the electrochemical deposition [31,38,39] and several kinds of aqueous solution methods [40–43] have been employed to prepare ZnO NWs. Although these methods can produce ZnO NWs by solution-based approaches at low temperature, tedious growth procedures or special substrates, such as GaN and Si-wafer are commonly required.

In this regard, in this work, we demonstrate a simple aqueous solution fabrication of the high density vertically aligned ZnO NWs on indium-doped tin oxide (ITO) substrates by selective-etching the dense ZnO rods. The method presented here offers several advantages, such as low growth temperature, catalyst-free, and potentially low-cost manufacturing. The ZnO NWs growth on ITO substrates at low-temperature hold promise for applications in both inverted PSCs and hybrid solar cells. As a preliminary application, the inverted PSCs based on ZnO NWs was constructed and investigated.

2. Experimental section

2.1. Materials

Zinc acetate dehydrate (99.0%), zinc nitrate hexahydrate (99.0%), 2-methoxy ethanol (99.0%), monoethanolamine (99.0%), hexamethylenetetramine (HMT, 99.0%) and potassium hydroxide (KOH) were purchased from Sigma-Aldrich and used as received without further purification. Regio-regular poly(3-hexylthiophene) (P3HT, 4002-E grade) was purchased from Rieke Metals, Inc. Methyl [6,6]-phenyl-C60-butyrate (PCBM, 99.0% purity) was purchased from American Dye Source Inc., Canada. The poly(3,4-ethylene-dioxylyene thiophene)-poly(styrene sulfonic acid) (PEDOT:PSS, Clevios 4083) was purchased from H.C. Starck. The ITO coated glasses (Colorado Concept Coatings LLC, 10–15 Ω sq^{-1}) were cleaned prior to use by ultrasonic agitation in a detergent solution, deionized (DI) water, acetone and isopropanol and then dried in air.

2.2. Preparation of ZnO nanowalls

ZnO nanowalls (NWs) were grown using a three-step method: spin-coating ZnO seeds on the ITO substrates, aqueous solution growth of ZnO rods and the selective-etching to form ZnO NWs. The ZnO seed layers were prepared by spinning coat a sol-gel with concentration of zinc acetate 0.1 M on the ITO substrates (10–15 Ω sq^{-1}), which has been described in our previous work [44]. Subsequently, the growth of ZnO rods were carried out by suspending the substrates coated with ZnO seed in a beaker filled with an equimolar aqueous solution of 0.1 M zinc nitrate hexahydrate ($\text{Zn}(\text{NO}_3)_2 \cdot 6\text{H}_2\text{O}$), and 0.1 M methenamine ($\text{C}_6\text{H}_{12}\text{N}_4$, HMT) at 75 °C for 3 h in water bath, the initial pH value of the solution was adjusted by adding CH_3COOH . The resultant substrates were removed from the solution, rinsed with DI water and then immersed into 0.3 M KOH aqueous solution at 80 °C for 15 min in water bath. Finally, the substrates were rinsed by DI water and then dried in oven at 80 °C for 1 h. The ZnO NWs, before used to prepare the inverted polymer solar cells, were further annealed at 350 °C for 20 min in air.

2.3. Device fabrication

Firstly, a PCBM interlayer was spin-coated from a dichloro-methane solution containing 20 mg ml^{-1} of PCBM onto the ZnO NWs at 1000 rpm for 30 s. After that, the samples were baked at 250 °C for 1 min to drive away residual solvent and assisting the PCBM contact with ZnO NWs. Huang et al. [23] demonstrated and explained that the PCBM layer between ZnO NW and active layer could improve the infiltration of the active polymer layer into the gaps between ZnO nanorods. Similarly, we introduced a layer of PCBM between ZnO NWs and active layer to help the infiltration of the active layer into ZnO NWs spacing. Secondly, the chlorobenzene blend solution of P3HT:PCBM containing (20 mg ml^{-1}) P3HT and (16 mg ml^{-1}) PCBM was spin coated onto the PCBM layer at 1000 rpm for 30 s. Then the samples were baked at 225 °C for 1 min to help the self-organization of P3HT, as well as driving away residual solvent and assisting the polymer infiltrate into the ZnO NWs [45]. Thirdly, a diluted PEDOT:PSS solution was subsequently spin-coated onto the P3HT:PCBM layer to form hole-transport layer. The devices were then baked at 120 °C for 10 min. At last, a 100 nm thick Ag top electrode film was deposited under a vacuum of 5×10^{-7} Torr. The size of the solar cells prepared on ITO substrates is $\sim 2.25 \text{ cm}^2$ and the size of each Ag electrode is $3.14 \times 10^{-6} \text{ m}^2$.

2.4. Characterization

The surface morphology of the specimens was characterized by scanning electron microscopy (SEM, Philips, JEOL JSM7000). The phase composition of the samples was characterized by X-ray diffraction (XRD, Philips PW 1830 diffractometer with Ni-filtered $\text{Cu-K}\alpha$ source ($\lambda = 1.5405 \text{ \AA}$) radiation). The J - V characteristics of the solar cells were tested in glovebox using a Keithley 2400 source measurement unit, and an Oriel Xenon lamp (450 W) coupled with an AM1.5 filter. A silicon solar cell certificated by the NREL was used as reference to calibrate the measurement condition. The light intensity of 100 mW cm^{-2} was used in this work.

3. Results and discussions

Fig. 1 shows the SEM images of the ZnO seed layer, as-grown dense ZnO rods, etched ZnO nanowalls (NWs) and the cross-section of the NWs. Fig. 1(A) reveals that the ZnO seed layer consists of uniform and densely packed particles with diameters around 10 nm. The high quality closely packed ZnO seed layer is crucial to achieve c -axis oriented ZnO rod arrays with controlled density and dimension through evolution selection growth in aqueous solution. Fig. 1(B) displays that the as-grown dense ZnO rods film consisting of dense and plate-like crystals, where the rods are packed so closely that most of the side walls of rods are grown together. Fig. 1(C) presents that the ZnO NWs are vertical to the substrate and the inset of a high magnified SEM image reveals the walls thickness are around 50 nm. Fig. 1(D) indicates the cross-section of the ZnO NWs.

In this work, we suggest that the growth of dense ZnO rods film should result from the following several reasons. Firstly, the small and densely packed particles in ZnO seed layer (Fig. 1(A)) will result in the growth of ZnO rods with high density. Secondly, both the high concentration (0.1 M) of Zn^{2+} in the aqueous solution and the low growth temperature (75 °C) will also lead to the growth of ZnO rods with increased diameters, and thus result in the growth of dense ZnO rods film. Thirdly, the low pH value is also an important factor for increasing crystal size of ZnO nanostructures grown from aqueous solution route. For the zinc nitrate hexahydrate–HMT aqueous solution system, the decrease of pH value produces a decrease in supersaturation and consequently a decrease of the nucleation

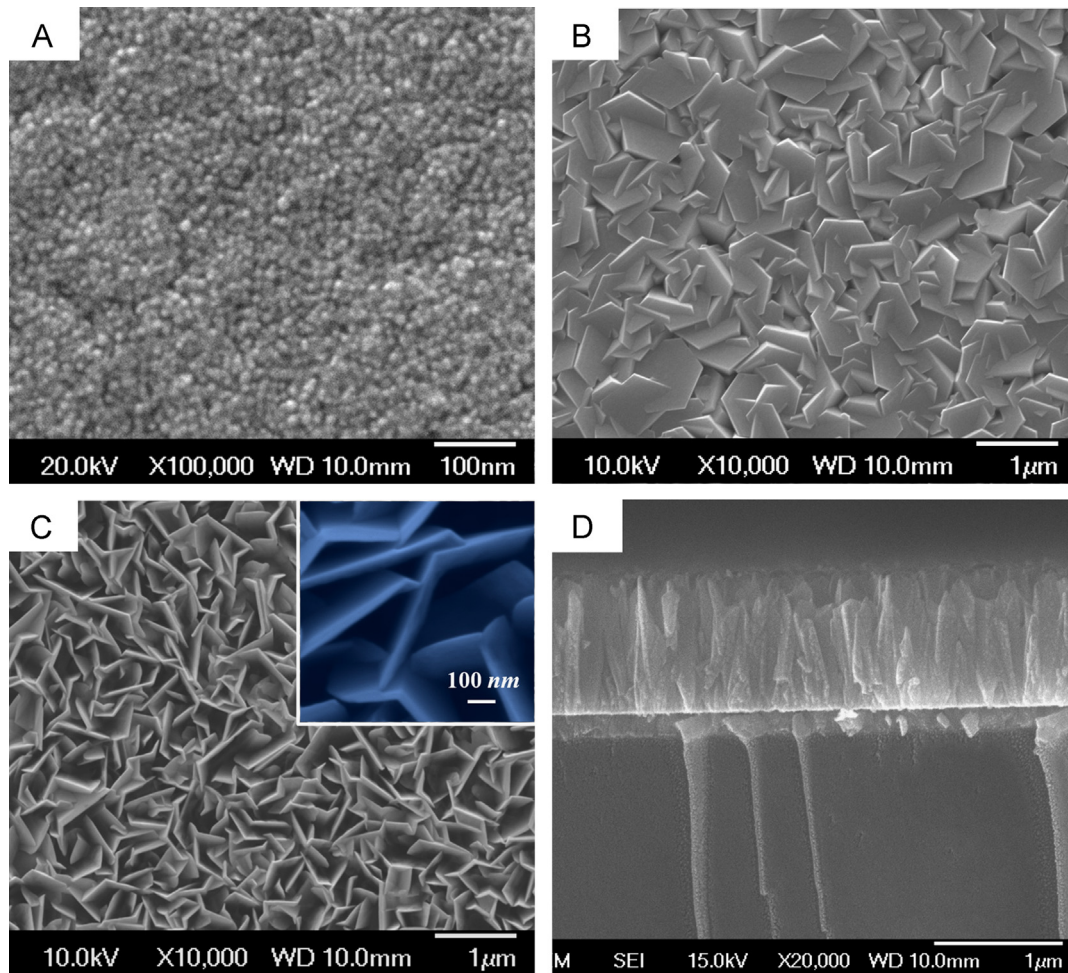


Fig. 1. SEM images of (A) ZnO seed layer, (B) as-grown dense ZnO rods, (C) etched ZnO nanowalls and the (D) cross-section of the nanowalls.

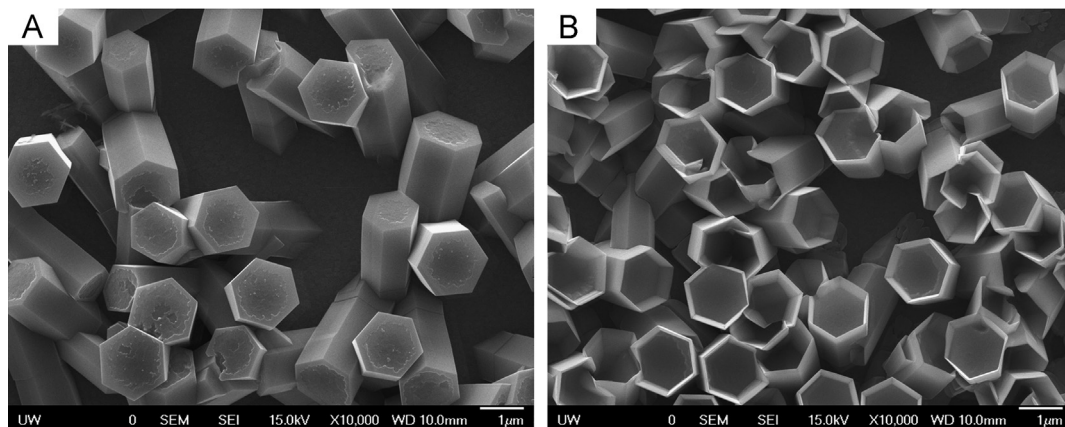


Fig. 2. SEM images of (A) as-grown ZnO rods and (B) etched ZnO nanotubes grown from solutions with initial pH value 5.9, the concentration of Zn^{2+} is 0.1 M and the growth temperature is 75 °C.

activation energy, and thus leads to the formation of ZnO crystals with bigger size [46,47]. As a result, the ZnO rods film consisting of dense and plate-like crystals were synthesized, where the rods are packed so closely that no individual rod exists and most of the side walls of rods are grown together.

As shown in Fig. 1(C), after etching in 0.3 M KOH at 80 °C for 15 min, the as-grown dense ZnO rods were transferred to ZnO NWs. The formation of ZnO NWs in this study may due to the defect-selective dissolution in (001) planes and along the *c*-axis caused by the preferential adsorption of OH^- on different crystal

faces [48,49]. During the etching process, the following reaction takes place [49]: $ZnO + 2OH^- \rightarrow ZnO^{2-} + H_2O$. In this study, the as-grown ZnO rods are so dense that most of the side walls of ZnO rods were grown together. Thus, during the selective etching in the (001) planes with the fastest rate of etching along [001] direction, the rods do not have all six side walls to form a complete tube structure, and thus the NWs structure were formed.

The ZnO rods growth in 0.1 M zinc nitrate hexahydrate and HMT aqueous solution with lower initial pH value was also investigated. Further decreasing the initial pH value of zinc nitrate

hexahydrate–HMT aqueous solution to ~ 5.9 led to the growth of ZnO rods with bigger size (Fig. 2(A)). In addition, the growth process with a lower pH value (~ 5.9) yielded no continuous rod array and part of ITO surface bared, it may be caused by the fact that at such a low pH value part of ZnO seeds will be dissolved [46,47]. Because the ZnO rods are complete and have all side walls, the ZnO nanotubes (ZNTs) (Fig. 2(B)) were derived by etching in 0.3 M KOH aqueous solution.

Fig. 3 shows that the XRD patterns of the as-grown ZnO rods and the etched nanowalls and nanotubes can be well indexed as wurtzite ZnO. High intensity of all diffraction peaks indicates a good crystallinity of the ZnO rods synthesized under the given experimental conditions. Moreover, for both kinds of rods, the intensity of (002) diffraction peak of ZnO rods is much stronger than that of other peaks, which indicates the rods have a preferred orientation along the [001] direction (*c*-axis). The intensity of (002) diffraction peaks of ZnO NWs and nanotubes are strongly decreased while other diffraction peaks changed slightly when compared to that of as-grown ZnO rods, suggesting that the (001)

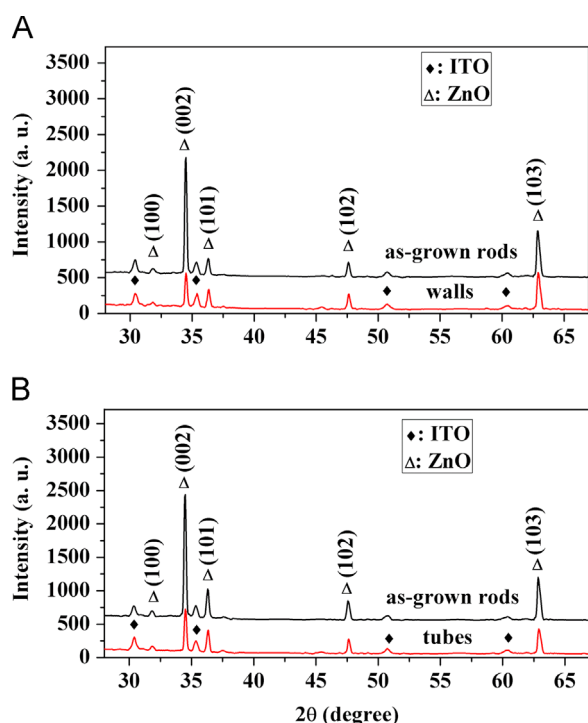


Fig. 3. XRD patterns of the as-grown ZnO rods and etched ZnO nanowalls and nanotubes grown from solutions with different initial pH values: (a) pH=6.4, and (b) pH=5.9.

plane area becomes smaller after etching in 0.3 M KOH aqueous solution. This is due to that the (001) planes of ZnO rods were selectively etched. This result is consistent with SEM observation that (001) planes disappear for ZnO NWs and nanotubes. Based on the abovementioned characterizations and discussions, the growth processes of ZnO NWs and nanotubes are illustrated in Fig. 4.

For the aqueous solution growth of ZnO, the growth temperature also plays an important role in affecting the morphology and crystallinity [47]. As shown in Fig. 5(A) and (B), ZnO rods grown at 85 °C and 95 °C possess smaller diameter than that grown at 75 °C. We also investigated the ZnO rods growth in lower concentration (0.005–0.05 M) of zinc nitrate hexahydrate and HMT aqueous solution at 95 °C (Fig. S1). It was found that both the diameter and density of ZnO rods decreased with increase of concentration of Zn^{2+} and HMT in the aqueous solution. These results prove that both the high concentration (0.1 M) of Zn^{2+} and the low growth temperature (75 °C) are the main reasons that lead to the growth of dense ZnO rods. In addition, Fig. 5(C) reveals that, after etched in 0.3 M KOH aqueous solution, the ZnO rods grown at 85 °C had been slightly etched to a bowl like structure, but no tube or wall structure was derived. The ZnO rods grown at 95 °C had been etched even less on the top of rods (Fig. 5(D)). The reason for this phenomenon may be ascribed to the better crystallinity and fewer defects in ZnO nanorods that are grown at relatively higher temperature [47,49]. Thus, no obvious defect-selective etching would occur from the (001) planes of rods along the *c*-axis.

The inverted polymer solar cells (PSCs) with a stacked structure of ITO/ZnO seed layer/ZnO NWs/PCBM/P3HT:PCBM/PEDOT:PSS/Ag (Fig. 6(a)) were fabricated and investigated. The thickness of the ZnO NW used in inverted devices is around 1 μm .

The current density–voltage (*J*–*V*) curves of the inverted devices with ZnO NW and nanorods are shown in Fig. 6(b). The devices with ZnO NWs yield an average PCE of 2.14%, with a short circuit current (J_{sc}), open circuit voltage (V_{oc}) and fill factor (*FF*) of 7.79 $mA\ cm^{-2}$, 0.55 V and 0.49, respectively. As a comparison, the devices based on ZnO rods, grown in 0.025 M zinc nitrate hexahydrate and HMT aqueous solution at 90 °C, show an average PCE of $\sim 2\%$ with a short circuit current (J_{sc}), open circuit voltage (V_{oc}) and fill factor (*FF*) of 8.41 $mA\ cm^{-2}$, 0.55 V and 0.43, respectively, tested under otherwise identical conditions and with all the same device process parameters. Although the difference in power conversion efficiency is not sufficient to prove the enhancement, the comparison between the devices with ZnO nanowalls and nanorods indicates that the two-dimensional structure of ZnO NW can effectively serve as an electrode for inverted polymer solar cells. However, the growth condition and the consequent surface chemistry, crystal perfection and morphology of ZnO NWs and NRs are different, so it remains inconclusive that ZnO NWs are better than ZnO NRs as a buffer layer in inverted polymer solar cells.

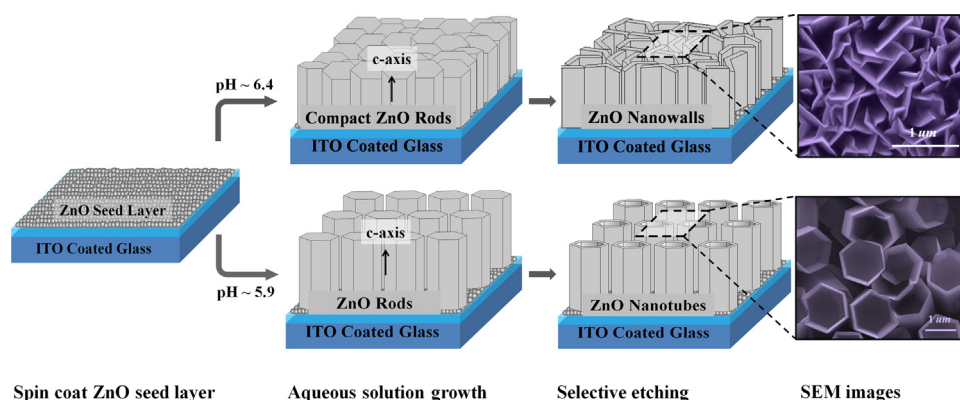


Fig. 4. The schematic diagram of the growth of ZnO nanowalls and nanotubes.

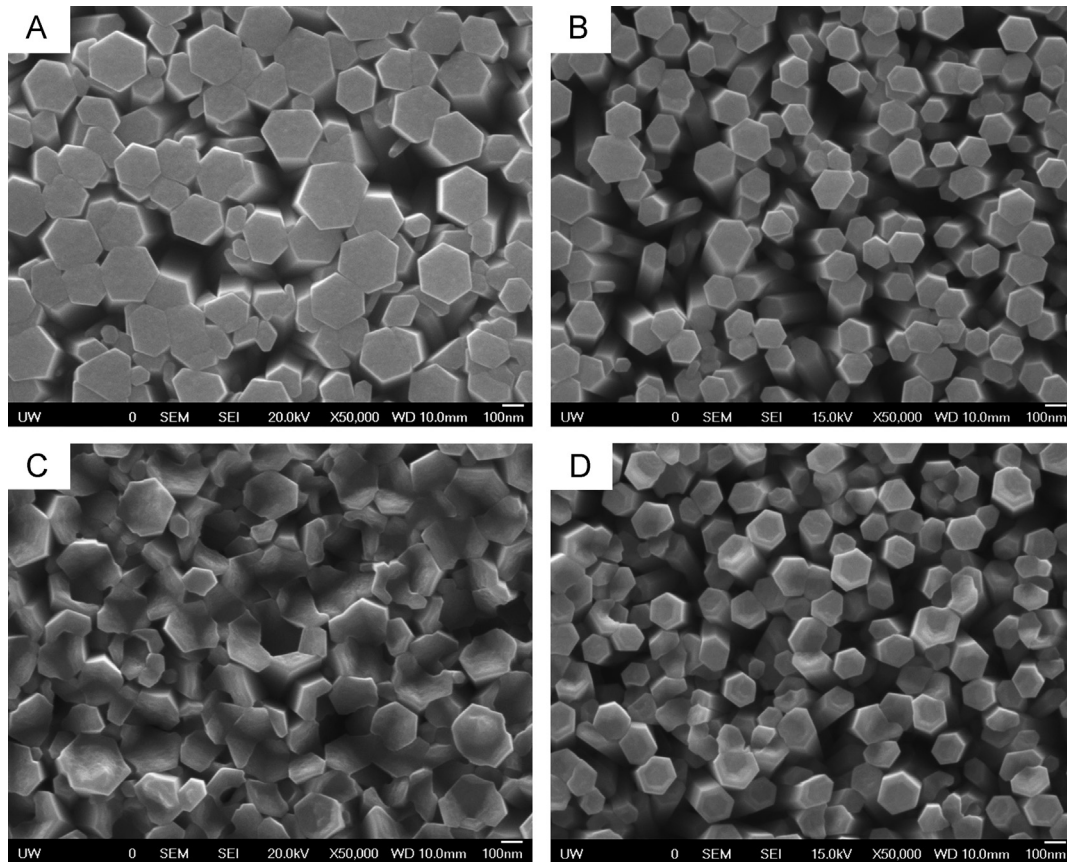


Fig. 5. SEM images of the as-grown ZnO rods grown at temperature of (A) 85 °C and (B) 95 °C, the concentration of Zn^{2+} was fixed at 0.1 M and the initial pH values of aqueous solution was ~ 6.4 . (C) and (D) are the SEM images of the ZnO nanostructures etched from (A) and (B), respectively.

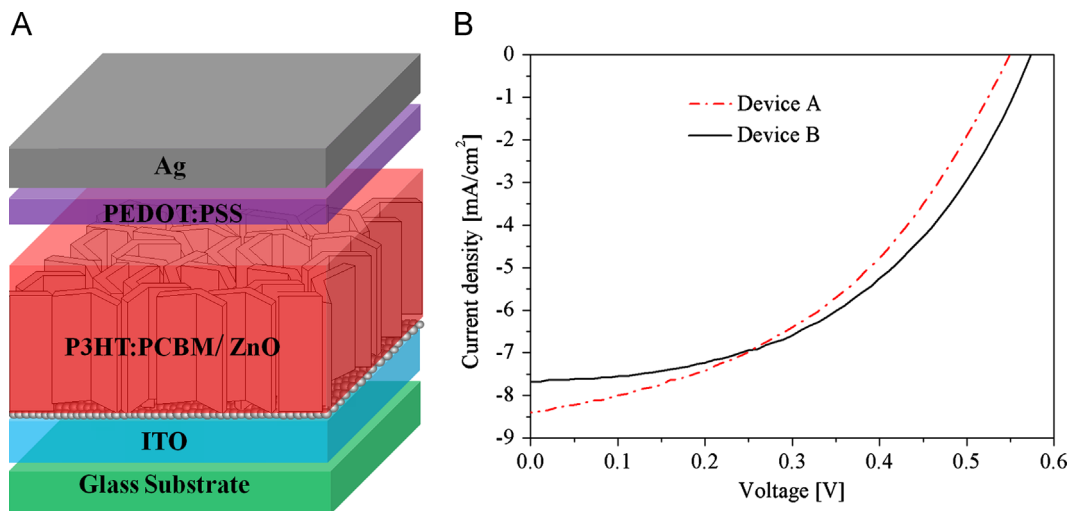


Fig. 6. (a) Schematic representation of the 3D nanostructured inverted device based on ZnO nanowalls, and (b) the J - V curves of device with (A) ZnO nanorods and (B) nanowalls.

Several literatures reported that the inverted PSCs with 1D ZnO nanowires/rods and P3HT:PCBM blend exhibited average PCEs over 3% [21–25]. In addition, the best inverted PSCs with dense and uniform ZnO films as buffer layer in our previous work yielded an average PCE of 3.3%, with a short circuit current (J_{SC}), open circuit voltage (V_{OC}) and fill factor (FF) of 9.59 mA cm^{-2} , 0.61 V and 0.56, respectively. Thus, we believe that the devices with ZnO NWs are far from their potential. The high density and vertically aligned ZnO NWs are expected to offer a large ZnO/P3HT:PCBM interface area to promote electron transfer and reduce the charge

recombination by supplying a direct pathway for fast electron transport to the charge-collecting electrode. It should be noted that the performance of inverted PSCs depends critically on the intimate contact between the active polymer and metal oxide [45]. The different morphology and surface area, in addition to the surface properties, would have impacts on the wetting and adhesion of polymer layers on ZnO NWs and on the charge transfers. The contact quality between ZnO and P3HT:PCBM can be reflected by the values of series resistance (R_S) and shunt resistance (R_{SH}) of the polymer solar cells. The average R_{SH} and R_S

calculated from the inverse slope of the J - V curves at $I=I_{SC}$ ($V=0$) and $V=V_{OC}$ ($I=0$) are $18.6\ \Omega\ \text{cm}^2$ and $950.0\ \Omega\ \text{cm}^2$, respectively [50]. Compared to that of the best inverted PSCs with intimate contact between the P3HT/PCBM and the dense and uniform ZnO films in our previous work [44], the R_{SH} of the devices with ZnO NWs is nearly the same while the R_S increased almost two times. It is known that the existence of contact resistance and charge recombination at the interface is the major reason of the increased R_S [19]. Thus, it is possible that the increase in R_S due to the PCBM: P3HT active layer infiltration and the contact quality between the ZnO NWs and P3HT:PCBM is far from good. However, the growth conditions for the nanowalls and dense films are different, so the resulting ZnO nanostructures are likely to have different level of crystal perfection (such as oxygen vacancies) and surface properties, which would affect the charge transfer at the interface and through the oxide. So it is difficult to conclude what the real impacts are on the power conversion efficiency. More research is needed to control, characterize and understand the impacts of the morphologies of ZnO nanostructures on the power conversion efficiency. We suggest that the power conversion efficiency would be much enhanced if the thickness and morphology of ZnO NWs are carefully tuned by controlling the etching process, and the interface modification is applied so that better infiltration of polymer into ZnO NWs can be achieved. Further studies are required to take the full advantages of the large surface area of ZnO nanowall electrode to achieve high efficiency inverted PSCs.

4. Conclusions

High-density and vertically aligned ZnO nanowalls have been fabricated on ITO coated glass substrate by a novel aqueous solution growth route at low-temperature. Both the SEM and XRD results revealed that the formation of nanowalls and nanotubes was due to selective dissolution of the (001) planes of ZnO rods films. It has been found that the resultant ZnO nanostructure is determined by the morphology of as-grown ZnO rods, which can be readily controlled by tuning initial pH value of the solution and growth temperature. The ZnO NWs have been explored as an electrode and a buffer layer in inverted polymer solar cells (PSCs). Although a power conversion efficiency of 2.14% is less impressive, the result shows that the aqueous growth ZnO NWs can effectively serve as an electrode for inverted polymer solar cells. Further studies are still required to take full advantage of the large surface area of ZnO NW electrode to achieve high efficiency inverted PSCs.

Acknowledgments

ZQL and RG are gratefully acknowledging the fellowships from China Scholarship Council. This work is supported in part by the National Science Foundation (DMR-1035196), and the University of Washington TGIF and the RRF Grants. Zhiqiang Liang and Rui Gao have contributed equally.

Appendix A. Supporting information

Supplementary data associated with this article can be found in the online version at <http://dx.doi.org/10.1016/j.solmat.2013.05.019>.

References

- [1] M.S. White, D.C. Olson, S.E. Shaheen, N. Kopidakis, D.S. Ginley, Inverted bulk-heterojunction organic photovoltaic device using a solution-derived ZnO underlayer, *Applied Physics Letters* (2006) 143517–143520.
- [2] F. Zhang, X. Xu, W. Tang, J. Zhang, Z. Zhuo, J. Wang, J. Wang, Z. Xu, Y. Wang, Recent development of the inverted configuration organic solar cells, *Solar Energy Materials and Solar Cells* 95 (2011) 1785–1799.
- [3] W. Cai, X. Gong, Y. Cao, Polymer solar cells: recent development and possible routes for improvement in the performance, *Solar Energy Materials and Solar Cells* 94 (2010) 114–127.
- [4] S.K. Hau, H.-L. Yip, A.K.Y. Jen, A review on the development of the inverted polymer solar cell architecture, *Polymer Reviews* 50 (2010) 474–510.
- [5] Y. Sun, J.H. Seo, C.J. Takacs, J. Seifert, A.J. Heeger, Inverted polymer solar cells integrated with a low-temperature-annealed sol-gel-derived ZnO film as an electron transport layer, *Advanced Materials* 23 (2011) 1679–1683.
- [6] Y.W. Heo, D.P. Norton, L.C. Tien, Y. Kwon, B.S. Kang, F. Ren, S.J. Pearton, J.R. LaRoche, ZnO nanowire growth and devices, *Materials Science and Engineering R: Reports* 47 (2004) 1–47.
- [7] J.-W. Kang, Y.-J. Kang, S. Jung, M. Song, D.-G. Kim, C. Su Kim, S.H. Kim, Fully spray-coated inverted organic solar cells, *Solar Energy Materials and Solar Cells* 103 (2012) 76–79.
- [8] D.C. Lim, W.H. Shim, K.-D. Kim, H.O. Seo, J.-H. Lim, Y. Jeong, Y.D. Kim, K.H. Lee, Spontaneous formation of nanoripples on the surface of ZnO thin films as hole-blocking layer of inverted organic solar cells, *Solar Energy Materials and Solar Cells* 95 (2011) 3036–3040.
- [9] J. Huang, Z. Yin, Q. Zheng, Applications of ZnO in organic and hybrid solar cells, *Energy & Environmental Science* 4 (2011) 3861–3877.
- [10] M.A. Ibrahim, H.-Y. Wei, M.-H. Tsai, K.-C. Ho, J.-J. Shyue, C.W. Chu, Solution-processed zinc oxide nanoparticles as interlayer materials for inverted organic solar cells, *Solar Energy Materials and Solar Cells* 108 (2013) 156–163.
- [11] T.-Y. Chu, S.-W. Tsang, J. Zhou, P.G. Verly, J. Lu, S. Beaupré, M. Leclerc, Y. Tao, High-efficiency inverted solar cells based on a low bandgap polymer with excellent air stability, *Solar Energy Materials and Solar Cells* 96 (2012) 155–159.
- [12] F.C. Krebs, J. Fyenbo, M. Jørgensen, Product integration of compact roll-to-roll processed polymer solar cell modules: methods and manufacture using flexographic printing, slot-die coating and rotary screen printing, *Journal of Materials Chemistry* 20 (2010) 8994–9001.
- [13] R. Søndergaard, M. Helgesen, M. Jørgensen, F.C. Krebs, Fabrication of polymer solar cells using aqueous processing for all layers including the metal back electrode, *Advanced Energy Materials* 1 (2011) 68–71.
- [14] F.C. Krebs, S.A. Gevorgyan, J. Alstrup, A roll-to-roll process to flexible polymer solar cells: model studies, manufacture and operational stability studies, *Journal of Materials Chemistry* 19 (2009) 5442–5451.
- [15] F.C. Krebs, T.D. Nielsen, J. Fyenbo, M. Wadstrom, M.S. Pedersen, Manufacture, integration and demonstration of polymer solar cells in a lamp for the “Lighting Africa” initiative, *Energy & Environmental Science* 3 (2010) 512–525.
- [16] R.R. Søndergaard, M. Hösel, F.C. Krebs, Roll-to-roll fabrication of large area functional organic materials, *Journal of Polymer Science Part B: Polymer Physics* 51 (2013) 16–34.
- [17] R. Thitima, C. Patcharee, S. Takashi, Y. Susumu, Efficient electron transfers in ZnO nanorod arrays with N719 dye for hybrid solar cells, *Solid-State Electronics* 53 (2009) 176–180.
- [18] Y. Hames, Z. Alpaslan, A. Kösemen, S.E. San, Y. Yerli, Electrochemically grown ZnO nanorods for hybrid solar cell applications, *Solar Energy* 84 (2010) 426–431.
- [19] M. Wang, Y. Li, H. Huang, E.D. Peterson, W. Nie, W. Zhou, W. Zeng, W. Huang, G. Fang, N. Sun, X. Zhao, D.L. Carroll, Thickness dependence of the MoO₃ blocking layers on ZnO nanorod-inverted organic photovoltaic devices, *Applied Physics Letters* (2011) 103305–103308.
- [20] Z. Hu, J. Zhang, Y. Liu, Z. Hao, X. Zhang, Y. Zhao, Influence of ZnO interlayer on the performance of inverted organic photovoltaic device, *Solar Energy Materials and Solar Cells* 95 (2011) 2126–2130.
- [21] K. Takanezawa, K. Tajima, K. Hashimoto, Efficiency enhancement of polymer photovoltaic devices hybridized with ZnO nanorod arrays by the introduction of a vanadium oxide buffer layer, *Applied Physics Letters* (2008) 063308–063311.
- [22] C.-Y. Chou, J.-S. Huang, C.-H. Wu, C.-Y. Lee, C.-F. Lin, Lengthening the polymer solidification time to improve the performance of polymer/ZnO nanorod hybrid solar cells, *Solar Energy Materials and Solar Cells* 93 (2009) 1608–1612.
- [23] J.-S. Huang, C.-Y. Chou, C.-F. Lin, Enhancing performance of organic-inorganic hybrid solar cells using a fullerene interlayer from all-solution processing, *Solar Energy Materials and Solar Cells* 94 (2010) 182–186.
- [24] J. Ajuria, I. Etxebarria, E. Azaceta, R. Tena-Zaera, N. Fernandez-Montcada, E. Palomares, R. Pacios, Novel ZnO nanostructured electrodes for higher power conversion efficiencies in polymeric solar cells, *Physical Chemistry Chemical Physics* 13 (2011) 20871–20876.
- [25] Y.-M. Sung, F.-C. Hsu, C.-T. Chen, W.-F. Su, Y.-F. Chen, Enhanced photocurrent and stability of inverted polymer/ZnO-nanorod solar cells by 3-hydroxyflavone additive, *Solar Energy Materials and Solar Cells* 98 (2012) 103–109.
- [26] N. Sekine, C.-H. Chou, W.L. Kwan, Y. Yang, ZnO nano-ridge structure and its application in inverted polymer solar cell, *Organic Electronics* 10 (2009) 1473–1477.
- [27] K.-S. Shin, H.-J. Park, B. Kumar, K.-H. Kim, S.-H. Kim, S.-W. Kim, Inverted organic solar cells with ZnO nanowalls prepared using wet chemical etching in a KOH solution, *Journal of Nanoscience and Nanotechnology* 12 (2012) 1234–1237.
- [28] S.W. Kim, S. Fujita, M.S. Yi, D.H. Yoon, Catalyst-free synthesis of ZnO nanowall networks on Si₃N₄/Si substrates by metalorganic chemical vapor deposition, *Applied Physics Letters* 88 (2006) 253114–253117.

- [29] S. Kim, et al., Epitaxial growth of ZnO nanowall networks on GaN/sapphire substrates, *Applied Physics Letters* 90 (2007) 033107–033110.
- [30] L. Chul-Ho, et al., Scalable network electrical devices using ZnO nanowalls, *Nanotechnology* 22 (2011) 055205–055211.
- [31] D. Pradhan, M. Kumar, Y. Ando, K.T. Leung, et al., Efficient field emission from vertically grown planar ZnO nanowalls on an ITO–glass substrate, *Nanotechnology* 19 (2008) 035603–035609.
- [32] R.-C. Wang, C.-C. Tsai, Efficient synthesis of ZnO nanoparticles, nanowalls, and nanowires by thermal decomposition of zinc acetate at a low temperature, *Applied Physics A* 94 (2009) 241–245.
- [33] Z. Yin, N. Chen, R. Dai, L. Liu, X. Zhang, X. Wang, J. Wu, C. Chai, On the formation of well-aligned ZnO nanowall networks by catalyst-free thermal evaporation method, *Journal of Crystal Growth* 305 (2007) 296–301.
- [34] X. Wang, Y. Ding, Z. Li, J. Song, Z.L. Wang, Single-crystal mesoporous ZnO thin films composed of nanowalls, *Journal of Physical Chemistry C* 113 (2009) 1791–1794.
- [35] F. Fang, D.X. Zhao, B.H. Li, Z.Z. Zhang, J.Y. Zhang, D.Z. Shen, The enhancement of ZnO nanowalls photoconductivity induced by CdS nanoparticle modification, *Applied Physics Letters* 93 (2008) 233115–233118.
- [36] M.M. Brewster, M.-Y. Lu, S.K. Lim, M.J. Smith, X. Zhou, S. Gradečak, The growth and optical properties of ZnO nanowalls, *Journal of Physical Chemistry Letters* 2 (2011) 1940–1945.
- [37] M.J. Alam, D.C. Cameron, Investigation of annealing effects on sol–gel deposited indium tin oxide thin films in different atmospheres, *Thin Solid Films* 420–421 (2002) 76–82.
- [38] D. Pradhan, S. Sindhvani, K. Leung, Parametric study on dimensional control of ZnO nanowalls and nanowires by electrochemical deposition, *Nanoscale Research Letters* 5 (2010) 1727–1736.
- [39] D. Pradhan, K.T. Leung, Controlled growth of two-dimensional and one-dimensional ZnO nanostructures on indium tin oxide coated glass by direct electrodeposition, *Langmuir* 24 (2008) 9707–9716.
- [40] M.Q. Israr, J.R. Sadaf, O. Nur, M. Willander, S. Salman, B. Danielsson, Chemically fashioned ZnO nanowalls and their potential application for potentiometric cholesterol biosensor, *Applied Physics Letters* 98 (2011) 253705–253708.
- [41] N.H. Alvi, S.M. Usman Ali, S. Hussain, O. Nur, M. Willander, Fabrication and comparative optical characterization of n-ZnO nanostructures (nanowalls, nanorods, nanoflowers and nanotubes)/p-GaN white-light-emitting diodes, *Scripta Materialia* 64 (2011) 697–700.
- [42] E.S. Jang, X. Chen, J.H. Won, J.H. Chung, D.J. Jang, Y.W. Kim, J.H. Choy, Soft-solution route to ZnO nanowall array with low threshold power density, *Applied Physics Letters* 97 (2010) 043109–043112.
- [43] D.-H. Kim, S.-D. Lee, K.-K. Kim, G.-S. Park, J.-M. Lee, S.-W. Kim, Free-standing ZnO nanorods and nanowalls by aqueous solution method, *Journal of Nanoscience and Nanotechnology* 8 (2008) 4688–4691.
- [44] Z. Liang, Q. Zhang, O. Wiranwetchayan, J. Xi, Z. Yang, K. Park, C. Li, G. Cao, Effects of the morphology of a ZnO buffer layer on the photovoltaic performance of inverted polymer solar cells, *Advanced Functional Materials* 22 (2012) 2194–2201.
- [45] D.C. Olson, Y.-J. Lee, M.S. White, N. Kopidakis, S.E. Shaheen, D.S. Ginley, J.A. Voigt, J.W.P. Hsu, Effect of polymer processing on the performance of poly (3-hexylthiophene)/ZnO nanorod photovoltaic devices, *Journal of Physical Chemistry C* 111 (2007) 16640–16645.
- [46] D. Chu, T. Hamada, K. Kato, Y. Masuda, Growth and electrical properties of ZnO films prepared by chemical bath deposition method, *Physica Status Solidi A* 206 (2009) 718–723.
- [47] D. Chu, Y. Masuda, T. Ohji, K. Kato, Formation and photocatalytic application of ZnO nanotubes using aqueous solution, *Langmuir* 26 (2009) 2811–2815.
- [48] L. Xu, Q. Liao, J. Zhang, X. Ai, D. Xu, Single-crystalline ZnO nanotube arrays on conductive glass substrates by selective dissolution of electrodeposited ZnO nanorods, *Journal of Physical Chemistry C* 111 (2007) 4549–4552.
- [49] G.W. She, X.H. Zhang, W.S. Shi, X. F. J.C. Chang, C.S. Lee, S.T. Lee, C.H. Liu, Controlled synthesis of oriented single-crystal ZnO nanotube arrays on transparent conductive substrates, *Applied Physics Letters* 92 (2008) 053111–053114.
- [50] K.-I. Ishibashi, Y. Kimura, M. Niwano, An extensively valid and stable method for derivation of all parameters of a solar cell from a single current–voltage characteristic, *Journal of Applied Physics* (2008) 094507–094513.